Highlights on Spanish Astrophysics X, Proceedings of the XIII Scientific Meeting of the Spanish Astronomical Society held on July 16 – 20, 2018, in Salamanca, Spain. B. Montesinos, A. Asensio Ramos, F. Buitrago, R. Schödel, E. Villaver, S. Pérez-Hoyos, I. Ordóñez-Etxeberria (eds.), 2019

The OTELO survey as morphological probe of galaxy evolution in the last 10 Gyr.

Jakub Nadolny[1,2] on behalf of the OTELO team

[1] Instituto de Astrofísica de Canarias, E-38205 La Laguna, Tenerife, Spain
[2] Universidad de La Laguna, Dept. Astrofísica, E-38206 La Laguna, Tenerife, Spain

Abstract

OTELO (OSIRIS Tunable filter Emission Line Objects) is an emission-line object survey covering a spectral range between 9070 and 9280Å in a window of reduced airglow emission. The first pointing of OTELO, in the Extented Groth Strip, consists of 36 tomographic slices sampled at 6Å, obtained with the red tunable filter of OSIRIS at the Gran Telescopio de Canarias. The limiting flux detecte of $\sim 5 \times 10^{-20}$ erg s^{-1} cm^2 makes it the deepest survey in its category to date. Taking advantage of OTELO survey characteristics in selection of Emission Line Systems (ELS) we aim to present qualitative and quantitative morphological analysis of ELS and non-ELS in a specific redshift ranges (given by specific emission line, e.g Hα at z$\sim$0.4 or [OIII] at z$\sim$0.8) up to z=2 using *HST*-ACS high resolution images. The source selection process, Sérsic profile fitting, the visual morphology classification and a preliminary results are presented.

1 Introduction

OTELO is a blind low-resolution ($\sim$700) 2D-spectroscopic survey defined in the spectral window centered at 9175Å and with width of 210Å. Using tomographic spectra scans of red tunable filter images we construct Pseudo-Spectra (PS). PS are then browsed in order to find sources which shows emission lines (Emission Line System or ELS) at specific redshift for given chemical spices. For details on the survey design, data reduction, etc. we refer to the OTELO presentation article [3], hereafter OTELO-I.

In this work we aim to provide morphological classification of all the OTELO sources up to z=2 regardless if these show emission or not in PS. Possibility to distinguish between ELS and non-ELS give us an opportunity to compare both samples down to low-end luminosity/mass regime (e.g. Hα sample at z$\sim$0.4 have stellar masses in the range of 10^7 and 10^{11} M$_\odot$, for details see Nadolny et al., in prep.).

2 Data

This work make a use of the OTELO data-products: OTELO catalogue, OTELO-deep image and Pseudo-spectra (PS). Shortly, OTELO catalogue contain multi-wavelength PSF-matched photometric data from X-rays to far-infrared recompiled by OTELO team. OTELO photometric redshift (`z_BEST_deepQ`, where `Q` is `Y` or `N`, see following sections) is estimated using `LePhare` code ([1], [6]) employing three different object libraries: galaxy, QSO and star. For details on OTELO data-products we refer to the OTELO-I where OTELO photometry, photometric redshifts, PS as well as auxiliary PSF-matched photometry, spectroscopic redshifts together with methods used are described. See also Bongiovanni Á. et al. contribution in this Proceedings.

The high-resolution *HST*-ACS F606W and F814W (hereafter V- and I-band, respectively) publicly available images were used to provide quantitative and visual morphological analysis. Images were retrieved from All-sky Extended Groth Strip International Survey (AEGIS) data base[1]. Both sets of images in V- and I-band (4 tiles per filter) were aligned to the same reference catalogue (i.e. the Canada-France-Hawaii Telescope Legacy Survey D3-25 i-band sources catalogue[2]) and in the same manner (using `ccxymatch` and `ccmap` IRAF tasks) as the OTELO data (see OTELO-I sec. 3.3).

3 Methods

In the morphological classification we decided to use solely aligned high-resolution images with average resolution of ∼0.15 arcsec (and native pixel scale of 0.03 arcsec/px). The OTELO-deep image is used only to get the OTELO detection radius in order to discriminate the contamination by unresolved in OTELO-deep image nearby sources which are detected in the *HST*-ACS data.

3.1 Sample selection

The sample selection process is based on the OTELO photometric redshift solutions. As described in OTELO-I, there are two sets of redshifts: with (`z_BEST_deepY`) and without (`z_BEST_deepN`) OTELO-deep photometry with estimated error σ(`z_BEST_deepQ`) defined as given in OTELO-I, sec. 5.6, equation 16. We decided to select sources with best redshift solution firstly with OTELO-deep photometry for sources with σ(`z_BEST_deepY`) $< 0.2 \times$ (1+`z_BEST_deepY`) and lower than σ(`z_BEST_deepN`). If these requirements are not met we select `z_BEST_deepN` solution, always if σ(`z_BEST_deepN`) $<0.2 \times$ (1+`z_BEST_deepN`). If neither solution is selected (due to σ(`z_BEST_deepQ`)), and the sources have redshift solution using QSO templates, we select firstly `z_QSO_deepY` and secondly `z_QSO_deepN`. In total we selected ∼6900 sources up to z=2 for the morphological analysis.

[1] `http://aegis.ucolick.org/mosaic_page.htm`

[2] See "T0007 : The Final CFHTLS Release" documentation at `http://terapix.calet.org/cplt/T0007/doc/T0007-doc.pdf`

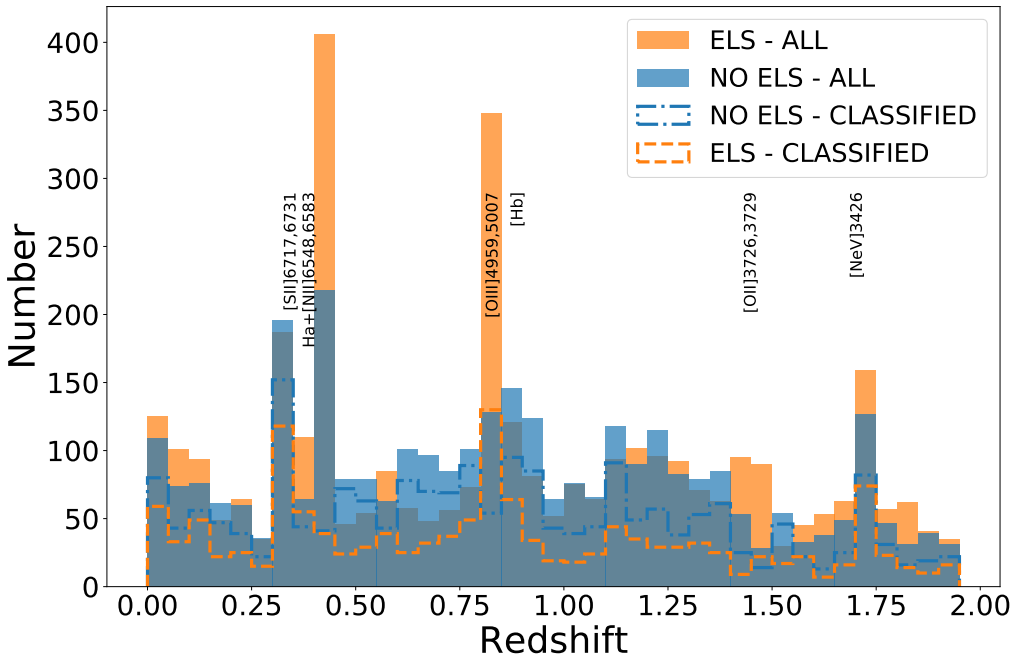

Figure 1: Redshift distribution of selected ELS (orange) and non-ELS (blue) up to z=2. The peak distributions at discrete redshifts (at ∼0.3, 0.4, 0.8, 1.4 and 1.75) shows sources with emission lines of specific chemical species which are redshifted to the spectral window of OTELO which is 210Å width and centered at 9175Å.

3.1.1 Emission Line Systems selection

ELS selection is done in a basis of automatic and visual inspection of PS and colour excess in the colour-magnitude diagram. Both methods are complementary and they are described in OTELO-I, sec 6.2 and Fig. 23. In total we have ∼3600 ELS and 3200 non-ELS. Resulting difference between sum of ELS and non-ELS and with the total selected described in previous section is due to star candidates in the field. Figure 1 shows redshift distribution of selected sources up z=2. Orange histogram shows objects selected as ELS, while blue shows non-ELS (orange and blue dashed lines show visually classified ELS and non-ELS, respectively).

3.2 Parametric classification

In order to provide parametric classification we use `IDL`-based `GALAPAGOS-2` software developed by MegaMorph group[3] [5]. We perform simultaneous fit (in V- and I-band) of single-Sérsic [9] profile of objects detected in I-band images. Together with Sérsic index we obtain other morphological parameters of the fitted model from `GALAPAGOS-2` (magnitude, effective radius, ellipticity, etc.). We perform also source extraction using `SExtractor` [2] software in dual, high-dynamical range mode with the same input parameters as given in GALAPAGOS-

[3] `https://www.nottingham.ac.uk/astronomy/megamorph/`

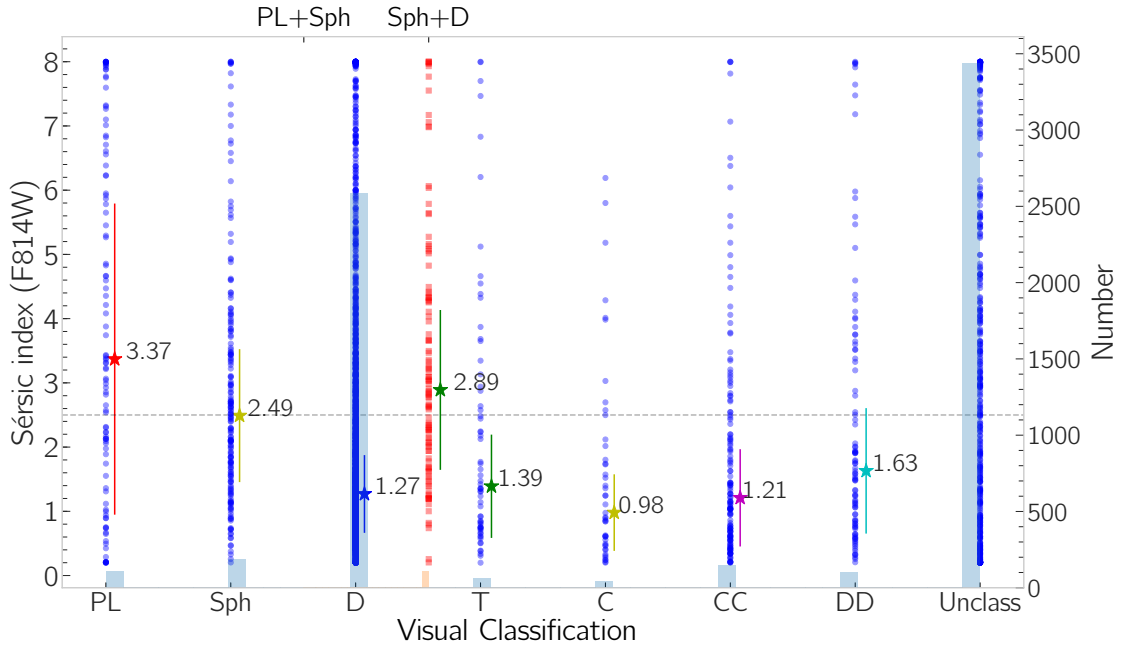

Figure 2: Visual classification correlation with Sérsic index. Blue points represent sources classified in one class, red squares show sources classified in mixed class. Star markers represent median Sérsic index per class with error bars calculated as median absolute deviation.

2 in order to get further information about detected sources (eg. flux radius at 20, 30, 50, 70 and 90% of the flux, magnitudes, etc.).

3.3 Visual classification

Visual classification is performed using MorphGUI [7], software developed originally for CANDELS. We modified the interface by extending basic morphological classes (Point-like, Spheroid and Disk) with Tadpole, Chain, Clumpy Cluster and Double following [4]. We decided to use this classification in order to take into account object diversity which is seen at higher redshifts.

4 Preliminary results

Figure 2 we resume both classifications: parametric and visual. We can notice that median Sérsic index n for early-type classes (Point-Like, Spheroid and mixed class Spheroid+Disk) is around and above $n = 2.5$. Sources classified as late-type objects (Disk, Tadpole, Chain, Clumpy Cluster, Double) are described with median n in range of $\sim$1 up to $\sim$1.6. This is expected behavior and observed in previous works (see e.g. [10]). In Figure 3 we show redshift distribution of sources in each morphological class. As we can notice the median

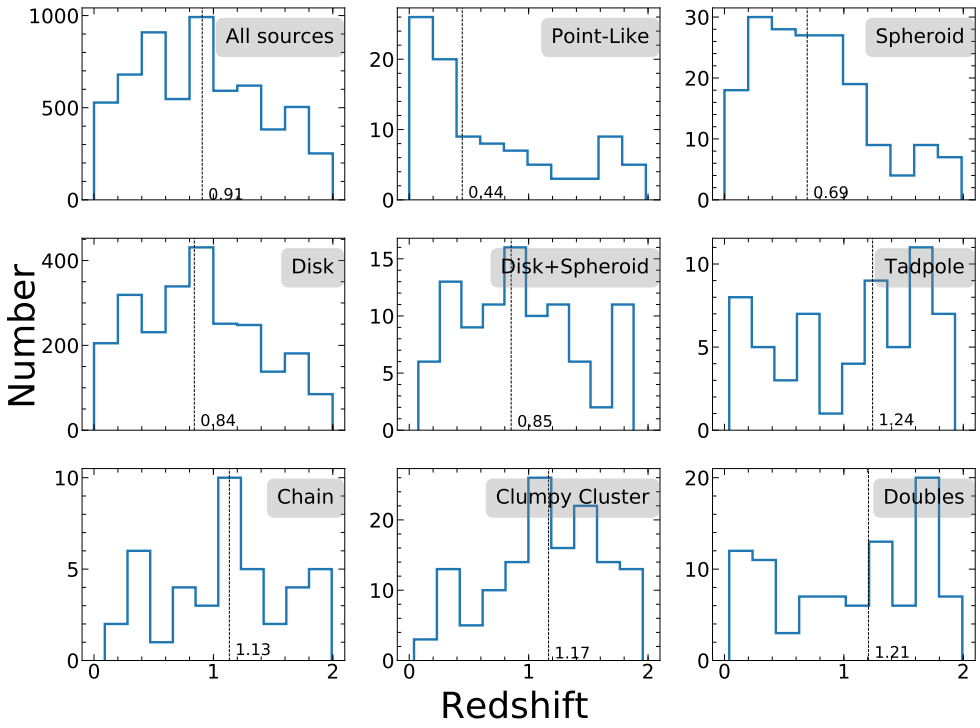

Figure 3: Redshift distribution per morphological class. Vertical dashed line shows median redshift per class.

redshift (vertical dashed line) for peculiar morphological classes (T, C, CC and DD) are higher than z=1. This behavior was observed also by [4] (see their Fig. 2).

5 Summary

In this work we provide qualitative and quantitative morphological classification for $\sim$ 7000 sources from OTELO catalogue up to z=2, regardless if these show or not emission line in PS. Automatic classification is done using `GALAPAGOS-2` software providing morphological parameters of analiytic model fitted to the sample sources. The dual, high-dynamical range model of `SExtractor` provide us with morphological parameters measured directly on the scientific image. Visual classification is carried out in order to disentangle the true nature of the sources (if possible due to the source size and brightness) taking advantage of high-resolution *HST*-ASC images. We decided to follow morphological classes given by [4] due to the fact that classical Hubble classification began to be not sufficient at higher redshifts where we can find sources which do not fit non of the Hubble sequence classes.

The main focus of the work – the comparison of ELS and non-ELS morphologies at specific redshifts where OTELO sees emission lines of different chemical spices – is in progress and we refer to Nadolny et al. (in prep.) for further analysis.

References

[1] Arnouts, S., Cristiani, S., Moscardini, L., et al. 1999, MNRAS, 310, 540

[2] Bertin, E., et al., 2002, ASPC, 281, 228B

[3] Bongiovanni, Á, et al. 2018, A&A, accepted 19/09/2018, `https://doi.org/10.1051/0004-6361/201833294`; OTELO-I

[4] Elmegreen, D. M., et al. 2007, ApJ, 658, 763E

[5] Häußler, B., et al. 2013, MNRAS, 430, 330

[6] Ilbert, O., Arnouts, S., McCracken, H. J., et al. 2006, A&A, 457, 841

[7] Kartaltepe, J. S., et al., ApJS, 221, 11K

[8] Newman, J. A., Cooper, M. C., Davis, M., et al. 2013, ApJS, 208, 5

[9] Sérsic, J. L., 1968

[10] Vika, M., et al. 2015, A&A, 577, A97